A Current Distribution for Broadside Arrays Which Optimizes the Relationship Between Beam Width and Side-Lobe Level*

C. L. DOLPH†

Summary—A one-parameter family of current distributions is derived for symmetric broadside arrays of equally spaced point sources energized in phase. For each value of the parameter, the corresponding current distribution gives rise to a pattern in which (1) all the side lobes are at the same level; and (2) the beam width to the first null is a minimum for all patterns arising from symmetric distributions of in-phase currents none of whose side lobes exceeds that level.

Design curves relating the value of the parameter to side-lobe level as well as the relative current values expressed as a function of side-lobe level are given for the cases of 8-, 12-, 16-, 20-, and 24-element linear arrays.

Introduction

FROM THE practical viewpoint, several things are desired of broadside antenna arrays. The beam should be as narrow as possible, the power gain a maximum, and the side lobes, if any, at a low level.

It is often a difficult matter to reconcile these demands. To illustrate, the gain may be made a maximum by feeding all of the point sources currents of equal magnitude and phase. Unfortunately, although it is true that this current distribution results in a narrow beam width, it also results in high side lobes of the order of 12 decibels down on the main lobe. In many applications it is more important to sacrifice some gain and beam width in order to achieve low-level side lobes. Several schemes have been suggested as a means of accomplishing this.

In particular, John Stone Stone[1] suggested that the point sources in an array of N elements be fed currents in phase with amplitudes proportional to the coefficients of a, b in the expansion $(a+b)^{N-1}$. The use of this so-called binomial expansion results in the total elimination of side lobes for spacings between the elements less than one-half wavelength but is in general impractical because of the increased beam width, loss of gain, and large current ratios demanded for large arrays.

S. A. Schelkunoff,[2,3] utilizing for the first time a correspondence between the nulls of the pattern and the roots of complex polynomials on the unit circle in the complex plane, was able to devise another scheme which did away, in part, with the above difficulties. By suitably spacing the roots of these polynomials on that portion of the unit circle traced out, he was able to derive many different types of pattern variation. In particular, by spacing these roots equally on the appropriate arc of the unit circle, he was always able to obtain an improvement in the side-lobe level over that of the uniform case for spacings less than one wave length. In this case, an algebraic identity led to formulas from which the current amplitudes and phases could be calculated. Since his treatment was carried out in the complex domain, it possessed the added advantage that it applied to both end-fire as well as broadside arrays. Although this method offers many advantages, it does not constitute a complete answer to this problem, since in certain applications the resulting improvement is inadequate.

This paper presents a third means of improving the pattern of linear arrays for the special broadside case in which the elements are fed in phase and are symmetrically arranged about the center of the array. The resultant current distribution across the array is based upon properties of the Tchebyscheff polynomials and offers, from the design standpoint, much greater control of the pattern. In particular, it possesses the following advantages:

(1) The current distribution can be calculated after either the side-lobe level or the position of the first null is specified.

(2) The current distribution is optimum in the sense that (a) if the side-lobe level is specified, the beam width is as narrow as possible (i.e., the number of degrees from the center of the beam to the first null is minimized); or (b) if the first null is specified, the side-lobe level is minimized.

(3) After either the side-lobe level or the position of the first null is specified, the position of the other nulls and of the side lobes can be found by simple calculation.

(4) All lobes other than the main beam and any other lobe arising from an in-phase condition of the same type as the main beam are at the same level.

(5) Detailed calculation of the pattern is unnecessary since the character of the pattern is completely known from the above properties.

General Pattern Considerations

The discussion of linear broadside symmetric arrays of equally spaced point sources differs slightly in detail depending upon whether the arrays contain $2N$ or $(2N+1)$ elements. In the first case there is no radiating element at the center 0 of the array while in the second

* Decimal classification: R325.112. Original manuscript received by the Institute, November 9, 1945; revised manuscript received, January 17, 1946.

† Formerly, Combined Research Group, Naval Research Laboratory, Washington, D. C.; now, Bell Telephone Laboratories, Murray Hill, N. J.

[1] John Stone Stone, United States Patents No. 1,643,323 and No. 1,715,433.

[2] S. A. Schelkunoff, "A mathematical theory of arrays," *Bell Sys. Tech. Jour.*, vol. 22, pp. 80–107; January, 1943.

[3] S. A. Schelkunoff, United States Patent No. 2,286,839.

case there is. These two different types with the appropriate values of I_n corresponding to the various point sources are shown in Figs. 1 and 2, respectively. In either case, let the center of the array 0 be taken as the phase reference point, let d denote the constant spacing

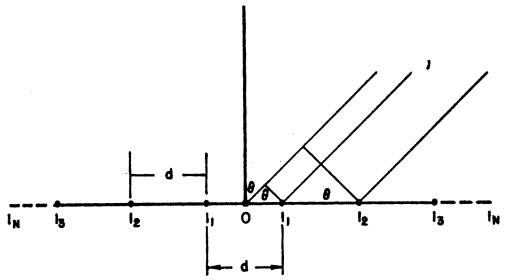

Fig. 1—Reference system for an array of $2N$ point sources.

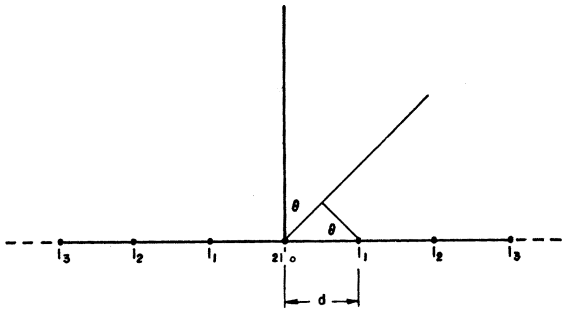

Fig. 2—Reference system for an array of $(2N+1)$ point sources.

between the point sources, let θ denote the angle between the direction of the field to distant point P and the normal to the array. Let I_n be proportional to the current fed into the point source located at a distance $(2n-1)d/2$ for Fig. 1 and at a distance of (nd) for Fig. 2. Let $2I_0$ denote the current fed into the center point source in Fig. 2. Then the field pattern of arrays of the type of Fig. 1 is well known to be proportional to

$$|E_{2N}(\theta)| = \left| \sum_{k=0}^{N-1} I_k \cos \left\{ \frac{(2k+1)}{2} \left(\frac{2\pi d}{\lambda} \right) \sin \theta \right\} \right| . \quad (1)$$

Similarly, the field pattern of arrays of the type of Fig. 2 is proportional to

$$|E_{2N+1}(\theta)| = \left| \sum_{k=0}^{N} I_k \cos \left\{ k \left(\frac{2\pi d}{\lambda} \right) \sin \theta \right\} \right| . \quad (2)$$

It must be emphasized again that (1) and (2) are valid only if all the currents are in phase along the array. Introducing the variable

$$u = \frac{d\pi}{\lambda} \sin \theta, \quad (3)$$

(1) and (2) become respectively

$$|F_{2N}(u)| = \left| \sum_{k=0}^{N-1} I_k \cos (2k+1)u \right| \quad (4)$$

and

$$|F_{2N+1}(u)| = \left| \sum_{k=0}^{N} I_k \cos (2ku) \right| . \quad (5)$$

In either case, the discussion of (4) and (5) can be reduced to the consideration of polynomials of a real variable $x=\cos u$ on the real interval $-1 \leqq x \leqq 1$. To obtain the polynomial form, use is made of the fact that

$$e^{inu} = (\cos nu + i \sin nu) = (\cos u + i \sin u)^n$$

from which it follows that

$$\cos nu = \cos^n u - \binom{n}{2} \cos^{n-2} u \sin^2 u + \binom{n}{4} \cos^{n-4} u \sin^4 u + \cdots \quad (6)$$

where

$$\binom{n}{k} = \frac{n!}{k!(n-k)!} .$$

If $\sin^2 u$ is replaced by $(1-\cos^2 u)$ it is apparent that $\cos nu$ is a polynomial of degree n in $x=\cos u$. It therefore follows that (4) and (5) are polynomials of degree $2N-1$ and $2N$ in x respectively, since they are merely sums of cosine polynomials. In fact, (4) is of the form $xP_{N-1}(x)^2$ where P_{N-1} is a polynomial of degree $(N-1)$ and (5) is of the form $Q_N(x^2)$ where Q_N is a polynomial of degree N.

Before obtaining explicit formulas for (4) and (5) in polynomial form, it is interesting to note a few fundamental properties which are consequences of this type of representation. The variable u is a universal parameter, the range of which is determined by the d/λ ratio. That is, if d/λ equals one, then the range of the variable u is clearly from $0 \leqq u \leqq \pi$. On the other hand, if d/λ is one half, then the range of u is $0 \leqq u \leqq \pi/2$. Since $\cos u$ in the range $0 \leqq u \leqq \pi/2$ is the negative of $\cos (\pi - u)$ in the range $\pi/2 \leqq u \leqq \pi$, it is clear that it is sufficient to compute either (4) or (5) in the range $0 \leqq u \leqq \pi/2$ and to use the recursion formula

$$|F(u)| = |F(\pi - u)| \quad (7)$$

corresponding to (4) and (5) respectively in order to obtain the pattern as a function of u over the range $0 \leqq u \leqq \pi$. Similar formulas are obvious if d/λ exceeds one. However, the range $0 \leqq u \leqq \pi/2$ corresponds to half-wave spacing while the range $0 \leqq u \leqq \pi$ corresponds to full-wave spacing. Since a change in frequency is equivalent to a change in spacing, it follows that different portions of the fundamental pattern arising from the range $0 \leqq u \leqq \pi/2$ occur as the frequency is changed. In particular, it becomes apparent that a large lobe equal to the main beam will arise at $\theta=90$ degrees for wavelength spacing. Since for wavelength spacing, $u=\pi/2$ corresponds to $\theta=30$ degrees while $u=\pi$ corresponds to $\theta=90$ degrees, the fundamental pattern of θ occurs first in the 0- to 30-degree range and is then repeated in reverse order in the 30- to 90-degree range on θ giving rise to a lobe at 90 degrees roughly twice as broad as (although equal in magnitude to) the main beam. Since the only way to reduce this 90-degree lobe is by the use of highly directive elements, it is in general

difficult to use spacing between the elements approaching one wavelength.

The introduction of the variable u makes clear the behavior of a broadside linear array over a band of frequencies provided that the current distribution remains unaltered as the frequency is shifted, a condition usually aimed at in design. That is, the portion of the fundamental pattern or multiples of it occurring in the range $0 \leqq u \leqq \pi/2$ merely changes as the frequency is shifted. In particular, if it is desired to calculate the performance of an array satisfying these conditions over a band of frequencies, it is only necessary to perform the calculations in terms of u over the basic range $0 \leqq u \leqq (\pi/2)$. The recursion formula (7), or others similar to it for values of d/λ greater than one, are then sufficient to give the pattern as a function of u corresponding to the d/λ ratio at the high end of the frequency band. Then it is only necessary to draw up a series of plots of (3) for the various d/λ ratios represented by the desired frequencies in the band and use this with the appropriate portion of the pattern as a function of u for the high end in order to obtain the complete pattern over the band.

In order to obtain explicitly polynomial representations in terms of $x = \cos u$ for (4) and (5), it is first necessary to verify that (6) implies that

$$\cos (2n+1)u = \sum_{m=0}^{n} A_{2m+1}{}^{2n+1} x^{2m+1} \tag{8}$$

where

$$A_{2m+1}{}^{2n+1} = (-1)^{n-m} \sum_{p=n-m}^{n} \binom{p}{p-n+m} \binom{2n+1}{2p} \tag{9}$$

and that

$$\cos 2nu = \sum_{m=0}^{n} A_{2m}{}^{2n} x^{2m} \tag{10}$$

where

$$A_{2m}{}^{2n} = (-1)^{n-m} \sum_{p=n-m}^{n} \binom{p}{p-n+m} \binom{2n}{2p}. \tag{11}$$

If (8) and (10) are inserted into (4) and (5) respectively, they become

$$G_{2N-1}(x) = \sum_{k=1}^{N} I_k \left\{ \sum_{m=1}^{k} A_{2m-1}{}^{2k-1} x^{2m-1} \right\}$$

and

$$G_{2N}(x) = \sum_{k=0}^{N} I_k \left\{ \sum_{m=0}^{k} A_{2m}{}^{2k} x^{2m} \right\}.$$

Since these last two equations involve finite double summations they can easily be rearranged to become respectively

$$G_{2N-1}(x) = \sum_{q=1}^{N} \sum_{k=q}^{N} I_k A_{2q-1}{}^{2k-1} x^{2q-1} \tag{12}$$

and

$$G_{2N}(x) = \sum_{q=0}^{N} \sum_{k=q}^{N} I_k A_{2q}{}^{2k} x^{2q}. \tag{13}$$

The difference between the lower limits in the outer summation sign of (12) and (13) arises because of the presence of a radiating element at the center of the array in the case of (13).

Equations (12) and (13) and their first derivatives with respect to u can be used to obtain the positions of the nulls and the side lobes of the radiation pattern of any symmetric in-phase broadside array. It is often true that the analytical processes involved are tedious if the number of elements in the array is large. The introduction of $y = x^2$ will materially simplify the analysis in all cases, however.

It is interesting to examine this type of representation for the case of the four-element array. This case exhibits all of the main points involved and is simple enough so that the mathematics does not present any difficulties. For a four-element array (4) becomes

$$F_4(u) = I_1 \cos u + I_2 \cos 3u.$$

Since $\cos 3u = 4\cos^3 u - 3\cos u$, this can be written as

$$G_3(x) = F_4(u) = x\{4I_2x^2 + (I_1 - 3I_2)\}$$

where $x = \cos u, \quad -1 \leqq x \leqq 1.$

The nulls therefore occur at $x = 0$ and at

$$x_0 = \pm \sqrt{\frac{3 - \frac{I_1}{I_2}}{4}}. \tag{14}$$

The position of the side lobes are given by the roots of $dG_3(x)/du = 0$. Thus the position of the main beam and the other in-phase lobes are given by

$$dx/du = -\sin u = 0$$

and the positions of the other side lobes by

$$\bar{x} = \pm \sqrt{\frac{3 - \frac{I_1}{I_2}}{12}}.$$

At these points $G_3(x)$ attains the value

$$|G_3(\bar{x})| = \frac{\sqrt{3}}{9} |I_2| \left| \left(3 - \frac{I_1}{I_2}\right)^{3/2} \right|.$$

The beam width is essentially given by the position of the first null which (14) determines. In this simple example, then, the beam width, the position of the side lobes, and the height or level of the side lobes are all functions of the same quantity, namely,

$$\left(3 - \frac{I_1}{I_2}\right).$$

The range of the ratio I_1/I_2 from $1 \leqq I_1/I_2 \leqq 3$ covers the range from the uniform distribution to the binomial. As the ratio increases over this range, it becomes apparent that the first null moves toward zero, so that the beam broadens and the side-lobe level drops until at the value of three the side lobes vanish altogether. It is also clear

that the beam can be made narrower than in the uniform case merely by choosing the range of I_1/I_2 from $0 \leqq I_1/I_2 \leqq 1$. The gain is of course a maximum for the uniform case.

It should be remarked again that, for larger arrays, it is in general impossible to devise physical means of achieving the range of current distribution from the uniform case to the binomial one because of the very large current ratios which become necessary in the latter case.

The Optimum Current Distribution

The distribution which will be deduced in this section has many properties in common with the distribution just discussed. As the taper is increased, the beam slowly broadens and the side-lobe level drops. It, however, possesses one great advantage: it is optimum in the sense that, once the side-lobe level is specified, the beam width (distance to first null) will be as small as possible; or, if the beam width is specified, the side-lobe level will be a minimum. Before demonstrating that this is always possible, it will be convenient to consider the nonnormalized Tchebyscheff polynomials. These are defined[4] by

$$T_n(z) = \cos (n \text{ arc cos } z). \tag{15}$$

To see that these are indeed polynomials of degree n in z, set $\phi = \text{arc cos } z$ and use (6). The nulls of these polynomials are given by the roots of $\cos n\phi = 0$, or by

$$\phi_k^0 = (2k-1)\pi/2n, \qquad k = 1, 2, \cdots, n. \tag{16}$$

Further, $T_n'(z) = 0$ whenever $\sin n\phi = 0$, or when

$$\bar{\phi}_k = k\pi/n, \qquad k = 1, 2, \cdots, n. \tag{17}$$

At the points $\bar{\phi}_k$, let $\bar{z}_k = \cos \bar{\phi}_k$. Then $|T_n(\bar{z}_k)| = 1$. If one uses (15) as the definition, then clearly $-1 \leqq z \leqq 1$. However, considered as a polynomial in z, $T_n(z)$ exists for all z, $-\infty \leqq z \leqq \infty$. Moreover, if $z > 1$, then $T_n(z)$ is monotonically increasing, and if $z < -1$, it is either monotonically increasing or decreasing depending upon whether n is even or odd. Furthermore, $T_n^{(k)}(z)$ can only vanish for any k, $(k = 1, 2, \cdots, n)$ in the interval between $-1 \leqq z \leqq 1$. This is obviously true by induction, since $T_n(z)$ has n roots in this interval and $T_n'(z)$ has $n-1$ roots contained within the n roots of $T_n(z)$, etc.

Equations (8), (9), (10), and (11) lead to the following expressions, respectively:

$$T_{2N-1}(z) = \sum_{q=1}^{N} A_{2q-1}{}^{2N-1} z^{2q-1}; \quad -\infty \leqq z \leqq \infty \tag{18}$$

$$T_{2N}(z) = \sum_{q=0}^{N} A_{2q}{}^{2N} z^{2q}; \quad -\infty \leqq z \leqq \infty. \tag{19}$$

Now if the range of z is restricted to $-z_0 \leqq z \leqq z_0$, then clearly (18) and (19) can be reduced to polynomials of the form of (12) and (13) by introduction of the scale contraction given by $x = z/z_0$, whereas before $x = \cos u$. Written in terms of x, $-1 \leqq x \leqq 1$, (18) and (19) become

$$T_{2N-1}(z_0 x) = \sum_{q=1}^{N} A_{2q-1}{}^{2N-1} z_0{}^{2q-1} x^{2q-1} \tag{20}$$

and

$$T_{2N}(z_0 x) = \sum_{q=0}^{N} A_{2q}{}^{2N} z_0{}^{2q} x^{2q}. \tag{21}$$

Now if (20) is equated to (12), the following set of equations is obtained:

$$\sum_{k=q}^{N} I_k A_{2q-1}{}^{2k-1} = A_{2q-1}{}^{2N-1} z_0{}^{2q-1}, \quad q = 1, \cdots, N.$$

These may be written in the form

$$I_q = \frac{1}{A_{2q-1}{}^{2q-1}} \left\{ A_{2q-1}{}^{2N-1} z_0{}^{2q-1} - \sum_{k=q+1}^{N} I_k A_{2q-1}{}^{2k-1} \right\}. \tag{22}$$

Similarly equating (21) to (13) yields

$$I_q = \frac{1}{A_{2q}{}^{2q}} \left\{ A_{2q}{}^{2N} z_0{}^{2q} - \sum_{k=q+1}^{N} I_k A_{2q}{}^{2k} \right\}. \tag{23}$$

It is clear that (22) and (23) can be solved for I_q, $q = 1, \cdots, N$ in terms of z_0 by a step-wise process starting from $q = N$.

Thus, for each value of z_0, the pattern as given by (12) or (13) can be made to agree with the pattern as given by (18) or (19). However, the characteristics of the latter expressions are completely known from the above discussion of the Tchebyscheff polynomials.

The parameter z_0 can be chosen in either of two ways: (1) the side-lobe level can be specified, or (2) the position of the first null can be specified.

In the first case, if the main-beam-to-side-lobe ratio is chosen to be $r/1$, it is necessary that z_0 satisfy the relation

$$T_M(z_0) = r; \qquad z_0 \geqq \cos (\pi/2M) \tag{24}$$

where

$M = 2N-1$ for an array of $2N$ elements
$= 2N$ for an array of $2N+1$ elements.

Once this value of z_0 has been determined and the current distribution computed from either (22) or (23), the pattern characteristics are completely known, since

(a) The side lobes are all equal and down on the main lobe in the ratio $1/r$.

(b) The nulls of the pattern are given by

$$u = \text{arc cos } [(\cos \phi_k^0)/z_0]; \quad k = 1, 2, \cdots, N \tag{25}$$

where ϕ_k^0 are given by (16) and u by (3).

(c) The positions of the side lobes are given by

$$u = \text{arc cos } [(\cos \bar{\phi}_k)/z_0]; \quad k = 1, 2, \cdots, N \tag{26}$$

where $\bar{\phi}_k$ is given by (17).

(d) The pattern between the nulls is given by

$$F(u) = \cos \{M \text{ arc cos } (z_0 \cos u)\} \tag{27}$$

or by

[4] Courant-Hilbert, "Methoden der Mathematischen Physik," vol. 1, pp. 75–76, Julius Springer, Berlin, 1931, and Interscience Publishers, Inc., New York, N. Y., 1943.

$$E(\theta) = \cos\left\{M \arccos\left[z_0 \cos\left(\frac{\pi d}{\lambda}\sin\theta\right)\right]\right\}.$$

In the second case, if the first null is specified as θ_0, it is necessary to compute x_1^0 from

$$x_1^0 = \cos u_1^0 = \cos\left(\frac{\pi d}{\lambda}\sin\theta_0\right)$$

and to choose z_0 from the relation

$$z_0 = \frac{1}{x_1^0}\cos\frac{\pi}{2M} \tag{28}$$

so that $$T_M(z_0 x) = T_M\left[\left(\cos\frac{\pi}{2M}\right) x/x_1^0\right]$$

will possess the necessary null at x_1^0. In this case, also, the pattern is completely characterized once the current distribution has been determined, since the main-beam-to-side-lobe ratio is $(\sum I_k):1$ and since the nulls, side-lobe positions, and pattern between the nulls are again given by (25), (26), and (27), respectively, when the value of z_0 from (28) is inserted.

The distribution by the solutions of (22) and (23) possesses the following important optimum property in addition to the above advantages: (1) *If the side-lobe level is specified, the beam width (i.e., the number of degrees to the first null) is minimized*; (2) *if the first null is specified, the side-lobe level is minimized.*

The proof of these statements is contained in the following theorem, which is clearly applicable to polynomials of the form (12) and (13).

Theorem:[4] Let $C(a)$ be a class of polynomials with real coefficients and of degree n having all of its roots in the interval $(-1, 1)$ such that

(1) If a polynomial $P(x)$ is in the class $C(a)$, then

$$P(x) = -P(-x) \quad \text{if } n \text{ is odd}$$
$$P(x) = P(-x) \quad \text{if } n \text{ is even}$$
$$P(1) = 1.$$

(2) If a polynomial $P(x)$ is in the class $C(a)$ and x_0 is its largest root (i.e., $|x_0|$ is a maximum among all the roots), then

$$|P(x)| \leqq a \quad \text{whenever} \quad |x| \leqq |x_0| \leqq 1.$$

Then

(1) There exists a polynomial $M(x)$ in $C(a)$ which maximizes $|x_0|$.

(2) The polynomial $M(x)$ is characterized by the fact that it just touches the lines $y = \pm a$ at $n-1$ points x_k within $|x| \leqq x_0$.

Specifically, $M(x) = aT_n(z_0 x)$ where z_0 satisfies the relations

$$T_n(z_0) = \frac{1}{a}; \qquad z_0 \geqq \cos\left(\frac{\pi}{2n}\right).$$

To prove this theorem, consider any polynomial in the class $C(a)$ which is not $M(x)$. Let x_0 be its largest root. Find y_0 from the relation

$$y_0 = \frac{\cos\left(\frac{\pi}{2n}\right)}{x_0} = z_1^0/x_0, \quad \text{where} \quad z_1^0 = \cos\left(\frac{\pi}{2n}\right)$$

and construct the polynomial [which may or may not belong to $C(a)$]

$$Q(x) = AT_n\left(\frac{z_1^0 x}{x_0}\right);$$

$Q(x)$ therefore also possesses x_0 as the largest root. Determine A so that $Q(1) = 1$; then $Q(-1) = -1$ if n is odd and $Q(-1) = 1$ if n is even. $Q(x)$ is therefore a polynomial which has the same largest root at $P(x)$ and which, since it is just a modified Tchebyscheff polynomial, is such that max $|Q(x)|$ is attained $n-1$ times between $-x_0 \leqq x \leqq x_0$.

Now it will be shown that

$$\max |Q(x)| < \max |P(x)|$$

when $|x| \leqq |x_0|$ so that $Q(x)$ belongs to $C(b)$ contained in $C(a)$. Assume the contrary; namely, that

$$\max |Q(x)| \geqq \max |P(x)| \tag{29}$$

when $|x| \leqq |x_0|$. Form the difference polynomial

$$D(x) = Q(x) - P(x)$$

which is, *at most*, of degree n. However, by construction of $Q(x)$

$$D(1) = 0, \qquad D(-1) = 0, \qquad D(x_0) = 0.$$

Let x_k, $k = 1, 2, n-1$, denote the $(n-1)$ points where $Q(x)$ attains its maximum value in the interval $|x| \leqq |x_0|$, and evaluate $D(x)$ at these points under the assumption (29), so that

$$D(x_1) \leqq 0, \; D(x_2) \geqq 0, \cdots, D(x_{n-1}) \lessgtr 0.$$

Thus $D(x)$ experiences $(n-2)$ changes in sign between $(-x_0, x_0)$ and consequently it must possess $(n-2)$ additional roots in this interval. This makes the total number of roots $(n+1)$, which is obviously impossible, since $D(x)$ is, at most, of degree n. Consequently, (29) is false and it therefore follows that

$$b = \max |Q(x)| < \max |P(x)| \leqq a \text{ when } |x| \leqq |x_0| < 1.$$

Consequently, unless $P(x)$ is $M(x)$, a polynomial $Q(x)$ can always be constructed possessing the same largest root as $P(x)$ and belonging to a class of polynomials $C(b)$ which is contained in the class $C(a)$. It therefore follows that $M(x)$ is the one polynomial in $C(a)$ which maximizes $|x_0|$.

Physically speaking, the improvement in beam width given by the above type of distribution results from the raising of the side lobes at wide angles to the level of those near the main beam. From a practical viewpoint, this is inconsequential for two reasons: (1) if the side lobes are sufficiently low in level everywhere, it is of no importance that they fall off with increasing angle, and (2) the primary patterns of many types of

radiating elements fall off with increasing angle so that the final wide-angle lobes would be at a lower level than those close to the beam.

Theoretically at any rate, (2) suggests that a still greater improvement in beam width for a given side-lobe level might be obtained by devising a current distribution for the point sources in which the side lobes increased in magnitude with increasing angle in just the right proportion so that the superposition of the array pattern and that of the primary radiator would result in an over-all pattern possessing side lobes at the desired constant level.

Estimation of Beam Width to Other Than the First Null

An estimate of the beam width to the half-power (3-decibel points) or to any other decibel point can be made readily if a plot of the side-lobe-level versus z_0 from (24) has been made over the appropriate range. Knowing the side-lobe level L in decibels, find from the curves of this type (see Appendix IV) the z_0 corresponding to this level. Also read from these curves the z_0' corresponding to $(L-R)$, where R is the number of decibels down on the maximum where the beam width is desired. The beam width in terms of u is then given by

$$u = \arccos (z_0'/z_0). \tag{30}$$

Again a plot of (3) can be used to give the beam width R decibels down on the maximum in terms of deviation from the normal to the array θ, or θ may be found directly from

$$\theta = \arcsin \left\{ \frac{\lambda}{\pi d} \arccos (z_0'/z_0) \right\}. \tag{31}$$

Examples of the Method

A linear, in-phase, symmetric array consisting of eight elements will first be used by way of illustration. In this case (4) becomes the following: (The absolute value sign may be omitted.)

$$F_8(u) = I_1 \cos u + I_2 \cos 3u + I_3 \cos 5u + I_4 \cos 7u.$$

From this (see Appendix I) it is readily deduced that

$$\begin{aligned} G_7(x) = x\{&64I_4x^6 + (16I_3 - 112I_4)x^4 \\ &+ x^2(4I_2 - 20I_3 + 56I_4) \\ &+ [I_1 - 3I_2 + 5I_3 - 7I_4]\}. \end{aligned} \tag{32}$$

Furthermore, from Appendix I, if $\phi = \arccos z$, then

$$T_7(z) = \begin{cases} z[64z^6 - 112z^4 + 56z^2 - 7] \text{ if } -\infty \leqq z \leqq \infty \\ \cos 7\phi \quad \text{if } |z| \leqq 1. \end{cases} \tag{33}$$

The following set of equations corresponding to (22) result when $G_7(x)$ is equated to $T_7(z_0x)$:

$$\begin{aligned} I_4 &= z_0^7 \\ I_3 &= 7I_4 - 7z_0^5 \\ I_2 &= 5I_3 - 14I_4 + 14z_0^3 \\ I_1 &= 3I_2 - 5I_3 + 7I_4 - 7z_0. \end{aligned} \tag{34}$$

Thus, once z_0 is determined from (24) or (28), the currents can be computed.

The pattern as a function of x is shown in Fig. 3 for $z_0 = 1.14$. This, as may be seen by referring to the plot of side-lobe level versus z_0 as given for an array of eight elements in Appendix IV, corresponds to a side-lobe level of 25.8 decibels.

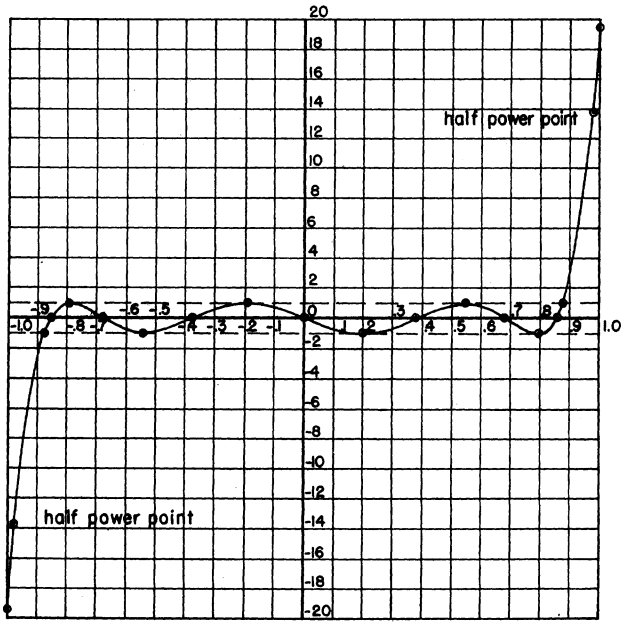

Fig. 3—$T_7(Z_0)$ versus x. "The optimum pattern" as a function of x for an 8-element array with a 25.8-decibel side-lobe level. $z_0 = 1.14$.

This same pattern, replotted as a function of u, is shown in Fig. 4.

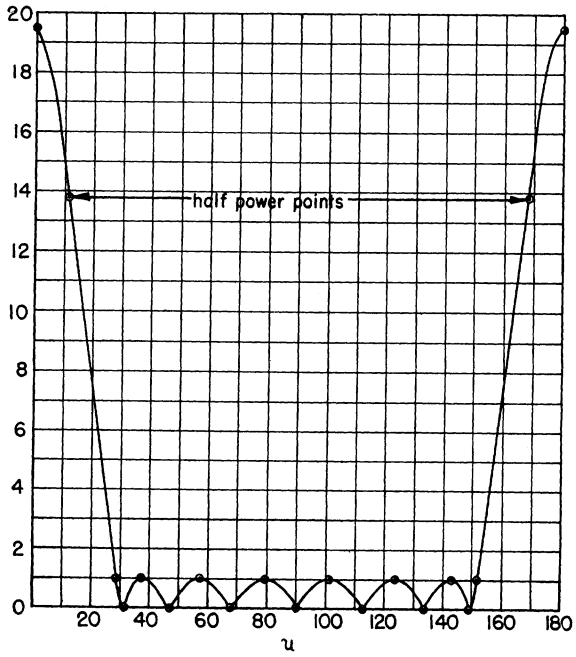

Fig. 4—$|F(u)| = |T_7(z_0 \cos u)|$ versus u for $z_0 = 1.14$. "The optimum pattern" as a function of u for an 8-element array with a 25.8-decibel side-lobe level.

Finally, this pattern is again replotted in terms of the physically measurable angle θ for the two spacing

wavelength ratios (d/λ) of one and one half in Fig. 5.

In all of these illustrations, only the circled points represent computed values. The data from which these

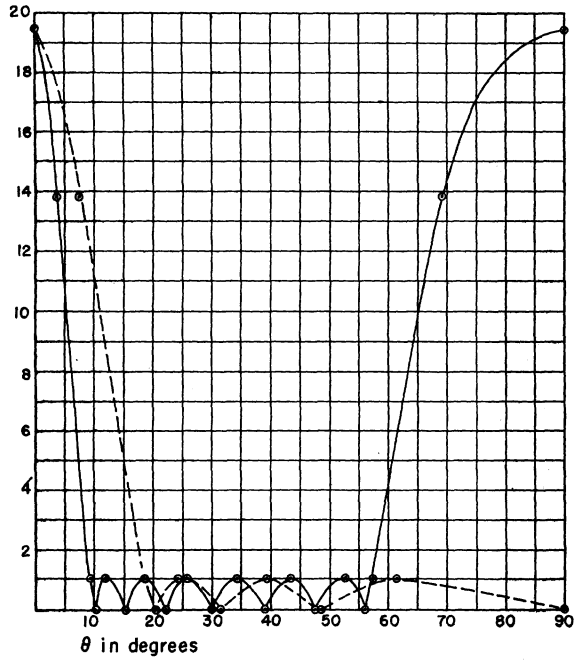

Fig. 5—$|E(\theta)| = |T_7[z_0 \cos \pi d/\lambda \sin \theta)]|$ versus θ for $z_0 = 1.14$. "The optimum pattern" as a function of θ for half-wave and full-wave spacing for an 8-element array with a 25.8-decibel side-lobe level.
——— $d/\lambda = 1$
------ $d/\lambda = \frac{1}{2}$

curves were drawn are summarized below in Table I, in which

rows one and two give the position of the nulls as a function of ϕ_k^0 from (16);

row three gives the computed values of the nulls as a function of $\cos \phi_k^0$;

row four gives the nulls, as function of x corresponding to the scale contraction associated with $z_0 = 1.14$;

row five gives the position of the nulls as a function of u as obtained from $x = \cos u$ and equation (3);

rows six and seven give the position of the nulls as a function of θ for $d/\lambda = 1$ and $d/\lambda = \frac{1}{2}$, respectively.

The second half of the table summarizes this same information for the position of the side lobes. In it, the starting point, row eight, is obtained from (17).

Column I gives the recursion formulas which were used to compute the table to the right of the first double vertical line in each half from the values to the left of it.

In addition to the above values, all the figures have plotted on them the maximum points, the estimated half-power points, and the extreme points where the beam attains the side-lobe level in its ascent to a maximum value.

The maximum points correspond to the fact that a 25.8-decibel side-lobe level corresponds to a main-beam-to-side-lobe-level ratio of 19.45.

The estimated half-power points of value (0.707) times (19.48) or 13.8, were located by means of (30), (31), and the curve from Appendix IV referred to above. That is, the value of $z_0' = 1.116$ corresponding to 22.8 decibels (3 decibels down on the main-beam-to-side-lobe-level ratio) was obtained from this curve.

TABLE I
8-ELEMENT ARRAY

			$z_0 = 1.14$						*Side-Lobe Level* = 25.8 *decibels*	
		A k	B 1	C 2	D 3	E 4	F 5	G 6	H 7	I
Null Positions	1	ϕ_k^0	$\frac{\pi}{14}$	$\frac{3\pi}{14}$	$\frac{5\pi}{14}$	$\frac{7\pi}{14}$	$\frac{9\pi}{14}$	$\frac{11\pi}{14}$	$\frac{13\pi}{14}$	
	2		12.85 degrees	38.6 degrees	64.3 degrees	90 degrees	115.7 degrees	141.4 degrees	167.15 degrees	$\cos \phi = -\cos(\pi - \phi)$
	3	$z_k^0 = \cos \phi_k^0$	0.9750	0.7815	0.4337	0	−0.4337	−0.7815	−0.9750	
	4	$x_k^0 = z_k^0/z_0$	0.854	0.685	0.380	0	−0.380	−0.685	−0.854	
	5	$u_k^0 = \text{arc cos } x_k^0$	31.35 degrees	46.7 degrees	67.5 degrees	90 degrees	112.5 degrees	133.3 degrees	148.65 degrees	$\lvert F(u)\rvert = \lvert F(\pi - u)\rvert$
	6 $d/\lambda = 1$	$\theta = \text{arc sin } \frac{\lambda u}{\pi d}$	10 degrees	15.1 degrees	22.1 degrees	30 degrees	38.7 degrees	47.4 degrees	55.7 degrees	
	7 $d/\lambda = \frac{1}{2}$	$\theta = \text{arc sin } \frac{\lambda u}{\pi d}$	20.4 degrees	31.3 degrees	48.6 degrees	90 degrees				
Side-Lobe Positions	8	$\bar{\phi}_k$	$\frac{\pi}{7}$	$\frac{2\pi}{7}$	$\frac{3\pi}{7}$	$\frac{4\pi}{7}$	$\frac{5\pi}{7}$	$\frac{6\pi}{7}$	0 / π	
			25.7 degrees	51.5 degrees	77.2 degrees	102.8 degrees	128.5 degrees	154.3 degrees	0/180 degrees	
	9	$\bar{z}_k = \cos \phi_k$	0.9011	0.6225	0.2215	−0.2215	−0.6225	−0.9011	+1 / −1	$\cos \phi = -\cos(\pi - \phi)$
	10	$\bar{x}_k = \frac{\bar{z}_k}{z_0}$	0.790	0.545	0.194	−0.194	−0.545	−0.790	0.876 / −0.876	
	11	$\bar{u}_k = \text{arc cos } \bar{x}_k$	36.8 degrees	56.9 degrees	78.8 degrees	101.2 degrees	123.1 degrees	143.2 degrees	28.8 degrees / 151.2 degrees	$\lvert F(u)\rvert = \lvert F(\pi - u)\rvert$
	12 $d/\lambda = 1$	$\theta = \text{arc sin } \frac{\lambda u}{\pi d}$	11.8 degrees	18.4 degrees	25.9 degrees	34.1 degrees	43.2 degrees	52.7 degrees	9.2 degrees / 57.1 degrees	
	13 $d/\lambda = \frac{1}{2}$	$\theta = \text{arc sin } \frac{\lambda u}{\pi d}$	24.2 degrees	39.2 degrees	61.1 degrees				18.7 degrees	

This locates the half-power points in terms of x at $x=\pm 1.116/1.14=\pm 0.9789$. Since $u=\text{arc cos } x$, this gives the location in terms of u at 11.8 and 168.2 degrees, respectively. For $d/\lambda=1$, these in turn correspond to $\theta=3.7$ and 69.2 degrees, respectively, giving an estimated total beam width of 7.4 degrees at the half-power points. For $d/\lambda=\frac{1}{2}$, the above values of u give a value of $\theta=7.5$ degrees, or an estimated total beam width at the half-power points of 15 degrees.

Finally, it is clear from the general theory that the side-lobe level will be reached at extreme points corresponding to $\phi=0, \pi$. The interpretation of these values in the x, u, and θ variables is carried through in column H in rows eight through thirteen.

It must be re-emphasized that, from the design viewpoint, all of the calculations tabulated in Table I are unnecessary, except perhaps the determination of the beam width at the half-power points. That is, practically, if the current distribution can be chosen to place the side lobe at an arbitrarily low level, it does not matter at all where they or the nulls occur. Table I is merely inserted as an aid to the understanding of the preceding theory, and for the sake of completeness.

Limiting Cases of the Optimum Distribution

It is interesting to examine the design equation (34) for the two limiting cases of unit z_0 and infinite z_0. In order to make this examination, it is first necessary to rewrite all of the currents as functions of z_0. If this is done, (34) becomes

$$\begin{aligned} I_4 &= z_0^7 \\ I_3 &= 7z_0^7 - 7z_0^5 \\ I_2 &= 21z_0^7 - 35z_0^5 + 14z_0^3 \\ I &= 35z_0^7 - 70z_0^5 + 42z_0^3 - 7z_0. \end{aligned}$$

Letting z_0 assume the value unity, all the I_k's vanish except I_4, which becomes unity, so that the pattern is proportional, by (3), to cos $7u$. In this case the side-lobe level is equal to that of the main beam. This result is, of course, expected because of the construction of this distribution.

In order to examine the case of infinite z_0, consider the set of equations obtained by dividing the above set by I_4.

$$\begin{aligned} I_4/I_4 &= 1 \\ I_3/I_4 &= 7 - 7/z_0^2 \\ I_2/I_4 &= 21 - 35/z_0^2 + 14/z_0^4 \\ I_1/I_4 &= 35 - 70/z_0^2 + 42/z_0^4 - 7/z_0^6. \end{aligned}$$

Letting z_0 approach infinity, the currents take on the ratios 1, 7, 21, 35. These are recognized as the binomial coefficients of the expansion $(a+b)^7$. In this case the pattern is well known to be proportional to $(\cos u)^7$ and contains no side lobes whenever u is restricted to the range $0 \leqq u \leqq (\pi/2)$. Thus, it is apparent that the above theory covers the entire range of side-lobe levels. It should be added that, whenever design equations are derived, these two limiting cases can be used as a convenient check.

Similarly, a seven-element array will be used as an illustration. In this case (5) becomes

$$F_7(u) = I_0 + I_1 \cos 2u + I_2 \cos 4u + I_3 \cos 6u.$$

Letting $x=\cos u$ and using (13), this can be written as

$$\begin{aligned} G_6(x) &= 32I_3x^6 + (8I_2 - 48I_3)x^4 \\ &\quad + (2I_1 - 8I_2 + 18I_3)x^2 + (I_0 - I_1 + I_2 - I_3), \end{aligned}$$

since

$$\begin{aligned} \cos 2u &= 2x^2 - 1 \\ \cos 4u &= 8x^4 - 8x^2 + 1 \\ \cos 6u &= 32x^6 - 48x^4 + 18x^2 - 1. \end{aligned}$$

Similarly, if $\phi=\text{arc cos } z$

$$\begin{aligned} T_6(z) &= 32z^6 - 48z^4 + 18z^2 - 1; \quad -\infty \leqq z \leqq \infty \\ &= \cos 6\phi; \quad -1 \leqq z \leqq 1 \end{aligned}$$

so that if the identification corresponding to (24) or (28) is made, the following design equations are obtained:

$$\begin{aligned} I_3 &= z_0^6 \\ I_2 &= 6I_3 - 6z_0^4 \\ I_1 &= 4I_2 - 9I_3 + 9z_0^2 \\ I_0 &= I_1 - I_2 + I_3 - 1. \end{aligned}$$

Since the construction of a table like the one given for the eight-element array proceeds almost as before and results in figures similar to 3, 4, and 5, no further details will be given here for the seven-element case. Moreover, because the author has been involved in the design of linear arrays of $2N$ elements exclusively, the detailed calculations and curves to be found in the appendixes are given for this case only.

It should be remarked that, if the current ratios are computed by formulas like (34) and those in Appendix III, and not normalized, then

$$20 \log \sum I_k$$

gives the side-lobe level in decibels at once.

Appendix I contains the Tchebyscheff polynomials of the form cos $(2n-1)\phi$ for $n=1, \cdots, 12$.

Appendix II gives the formula for $G_{23}(x)$ for an array of 24 elements. The appropriate formulas for shorter arrays of $2N$ elements can be deduced instantly merely by setting the excess I_k equal to zero.

Appendix III contains the design equations similar to (34) for this type of distribution of arrays consisting of 12, 16, 20, and 24 elements.

Appendix IV gives design curves for arrays of this type consisting of 8, 12, 16, 20, and 24 elements. These curves are given for a range of 26- to 40-decibel side-lobe level and show

(1) the variation of the side-lobe level with z_0;

(2) the variation of the currents as a function of the side-lobe level;

(3) the reduction in power gain from a uniform array consisting of the same number of elements as a function

of the side-lobe level for 8-, 12-, and 24-element arrays under the assumption that the mutual impedances between the elements are zero.

In this, the power-gain reduction from a uniform array is given by the well-known and easily derivable formula

$$G = \frac{\left(\sum_1^N I_k\right)^2}{N\left(\sum_1^N I_k^2\right)}$$

for symmetrical arrays of $2N$ elements.

If the mutual impedances between the elements are small but not zero, the above formula is still a good approximation to the gain reduction that can be expected.

Comparison of the Beam Width of a Uniform Array and the Tchebyscheff Distribution

If all the I_k's are equal, then it is easily shown that (4) can be written (for an array of $2N$ elements) as

$$F(u) = \frac{1}{2}\frac{\sin 2Nu}{\sin u} = \sum_{k=0}^{N-1} \cos(2k-1)u.$$

The first null of this is therefore given by

$$\sin 2Nu = 0, \quad \text{or} \quad u = \pi/2N.$$

The corresponding first null for a Tchebyscheff distribution is given by

$$u = \text{arc cos}\left\{\frac{1}{z_0}\cos\frac{\pi}{2(2N-1)}\right\}$$

so that, as in the general case, z_0 can be chosen so as to make the first null either equal to that of the uniform case or smaller than that.

A moment's reflection therefore shows that, when the side-lobe level starts to approach that of the uniform case, inversions must necessarily appear in the Tchebyscheff distribution. This explains the fact that the curves in Appendix IV sometimes cross.

Rectangular Arrays

For the purpose of the ensuing discussion it is convenient to locate a co-ordinate system at the center 0 of the outer rectangle enclosing the array. Let the x, y axes of this co-ordinate system be parallel to the sides of the rectangle. Let the *constant* spacing between the elements in the x, y directions be (a), (b), respectively. Assume that there is a radiating element at 0. With these conventions, the various radiating elements will be located at points (pa, qb) where p, q take on positive and negative integral values including zero. In the general case, these radiating elements can be fed with currents possessing arbitrary amplitudes and phase with respect to the element at 0. However, if the distribution of currents in any column, row is proportional to that of any other column, row respectively, then the 2-dimensional array factor S_{xy} is the product of two 1-dimensional array factors S_x and S_y. Here S_x may be taken for convenience as the array factor arising from the distribution of currents in the radiating elements along the x axis. Similarly, S_y may be thought of as arising from the distribution of currents in the radiating elements along the y axis.

If the angles are as in Fig. 6, and if α_p, β_q represent any phase shift which may be introduced in radiating

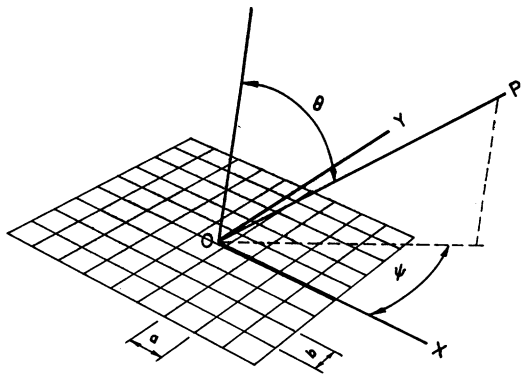

Fig. 6—Reference system for a two-dimensional array of point sources.

elements located at $(pa, 0)$ and $(0, qb)$, respectively, then the 2-dimensional array factor S_{xy} for a rectangular array possessing $2M+1$ elements parallel to the x axis and $(2N+1)$ elements parallel to the y axis is given by

$$S_{xy} = \left|\left\{\sum_{p=-M}^{M} A_p \exp\left[jp\frac{2\pi}{\lambda}a\sin\theta\cos\psi + j\alpha_p\right]\right\} \left\{\sum_{q=-N}^{N} B_q \exp\left[jq\frac{2\pi}{\lambda}b\sin\theta\sin\psi + j\beta_q\right]\right\}\right|. \quad (35)$$

In order to apply the above 1-dimensional theory to either S_x or S_y, the factors of S_{xy}, it is merely necessary to set all the α_p's, β_q's, respectively, equal to zero and to impose the conditions that

$$A_p = A_{(-p)}; \qquad \psi = 0$$

or that

$$B_q = B_{(-q)}; \qquad \psi = \pi/2.$$

If this is done in the case of S_x, as would be convenient if a sharp azimuth pattern were desired, it would become

$$S_x = \left|A_0 + 2\sum_{p=1}^{M} A_p \cos\left(2p\frac{\pi}{\lambda}a\sin\theta\right)\right|.$$

Letting $v = (\pi/\lambda)a\sin\theta$, this last equation becomes

$$S_x = \left|A_0 + 2\sum_{p=1}^{M} A_p \cos(2pv)\right|. \quad (36)$$

Equation (36) is recognized as being in the same form as (5) and therefore the same design procedure applicable there should be used here. If a sharp vertical pattern is desired, S_y can be treated in a similar fashion. On the other hand, if a different type of pattern is desired, the usual techniques can be applied to determine the appropriate values of B_q.

In either event, the pattern will be given by (35). The actual current to be fed into the element located at

(pa, qb) is of course $A_pB_qe^{j(\alpha_p+\beta_q)}$ in all cases.

It is unfortunate, perhaps, that the design curves contained in the appendix were not computed for (36) and hence cannot be used to sharpen the pattern in one or both directions. However, if the column and the row of radiators passing through the center 0 is struck out, as well as every other column and row, then the resulting expressions are just those computed in the appendix. Explicitly, if

$$A_0 = 0 \qquad B_0 = 0$$

$$A_{2p} = 0 \qquad B_{2q} = 0 \qquad p = 1, 2, \cdots, M \qquad q = 1, 2, \cdots, N$$

then the separation between the elements along the x, y directions is, respectively, $(2a)$ and $(2b)$. Let these be denoted by (d) and (d'), respectively. Then if

$$w = \frac{\pi d}{\lambda} \sin \theta$$

and it is desired to apply the theory to the x direction, so that $\alpha_p = 0$, equation (36) becomes

$$\frac{S_x}{2} = \left| \sum_{p=1}^{M} A_p \cos (2p - 1)w \right|.$$

This is recognized as of the same form as (4) so that the curves contained in the appendixes are applicable. S_y can be treated similarly or again made to conform with any other desired distribution.

Experimental Verification

The preceding theory has been utilized in the design of several linear arrays with excellent results.

Specifically, 12- and 24-element arrays of directive elements with $(4/5\lambda)$ spacing at the mid-band frequency have been successfully built and made to operate over a ± 10 per cent band with a 26-decibel side-lobe level. Both of the arrays were designed for a side-lobe level of 32 decibels and at the high end of the frequency band the 12-element array actually possessed a side-lobe level of 31 decibels. The performance of the 24-element array, while excellent, did not show as close an agreement with the predicted performance because of its greater complexity.

The beam widths to the half-power points were of the order of 6 degrees and 3 degrees, respectively, at the mid-band frequency and showed a total variation of about 1 degree over the band.

This experience, while admittedly limited, is sufficient to indicate that the above theory can be used successfully as a basis for design provided that a safety factor of from 3 to 5 decibels is allowed in the side-lobe level. This discrepancy between theory and practice is partly due to constructional difficulties and partly due to the finite size of the reflector behind the point sources in a physical array.

Appendix I

The nonnormalized Tchebyscheff polynomials

$$\cos (2n - 1)\theta, \quad n = 1, 2, \cdots, 10$$

$$\cos \theta = x$$

$$\cos 3\theta = x\{4x^2 - 3\}$$

$$\cos 5\theta = x\{16x^4 - 20x^2 + 5\}$$

$$\cos 7\theta = x\{64x^6 - 112x^4 + 56x^2 - 7\}$$

$$\cos 9\theta = x\{256x^8 - 576x^6 + 432x^4 - 120x^2 + 9\}$$

$$\cos 11\theta = x\{1024x^{10} - 2816x^8 + 2816x^6 - 1232x^4 + 220x^2 - 11\}.$$

$$\cos 13\theta = x\{4096x^{12} - 13{,}312x^{10} + 16{,}640x^8 - 9984x^6 + 2912x^4 - 364x^2 + 13\}$$

$$\cos 15\theta = x\{16{,}384x^{14} - 61{,}440x^{12} + 92{,}160x^{10} - 70{,}400x^8 + 28{,}800x^6 - 6048x^4 + 560x^2 - 15\}$$

$$\cos 17\theta = x\{65{,}536x^{16} - 278{,}528x^{14} + 487{,}424x^{12} - 452{,}608x^{10} + 239{,}360x^8 - 71{,}808x^6 + 11{,}424x^4 - 816x^2 + 17\}$$

$$\cos 19\theta = x\{262{,}144x^{18} - 1{,}245{,}184x^{16} + 2{,}490{,}368x^{14} - 2{,}723{,}840x^{12} + 1{,}770{,}496x^{10} - 695{,}552x^8 + 160{,}512x^6 - 20{,}064x^4 + 1140x^2 - 19\}$$

$$\cos 21\theta = x\{1{,}048{,}576x^{20} - 5{,}505{,}024x^{18} + 12{,}386{,}304x^{16} - 15{,}597{,}568x^{14} + 12{,}042{,}240x^{12} - 5{,}870{,}592x^{10} + 1{,}793{,}792x^8 - 329{,}472x^6 + 33{,}264x^4 - 1540x^2 + 21\}$$

$$\cos 23\theta = x\{4{,}194{,}304x^{22} - 24{,}117{,}248x^{20} + 60{,}293{,}120x^{18} - 85{,}917{,}696x^{16} + 76{,}873{,}728x^{14} - 44{,}843{,}008x^{12} + 17{,}145{,}856x^{10} - 4{,}209{,}920x^8 + 631{,}488x^6 - 52{,}624x^4 + 2024x^2 - 23\}.$$

Check:

If $x = 1$, $\cos n\theta = 1$.

Appendix II

24-Element Array

$$G_{23}(x) = x\{4{,}194{,}304I_{12}x^{22} + (-24{,}117{,}248I_{12} + 1{,}048{,}576I_{11})x^{20} + (60{,}293{,}120I_{12} - 5{,}505{,}024I_{11} + 262{,}144I_{10})x^{18} + (-85{,}917{,}696I_{12} + 12{,}386{,}304I_{11} - 1{,}245{,}184I_{10} + 65{,}536I_9)x^{16} + (76{,}873{,}728I_{12} - 15{,}597{,}568I_{11} + 2{,}490{,}368I_{10} - 278{,}528I_9 + 16{,}384I_8)x^{14} + (-44{,}843{,}008I_{12} + 12{,}042{,}240I_{11} - 2{,}723{,}840I_{10} + 487{,}424I_9 - 61{,}440I_8 + 4096I_7)x^{12} + (17{,}145{,}856I_{12} - 5{,}870{,}592I_{11} + 1{,}770{,}496I_{10} - 452{,}608I_9 + 92{,}160I_8 - 13{,}312I_7 + 1024I_6)x^{10}$$

$$+ (-4{,}209{,}920I_{12} + 1{,}793{,}792I_{11} - 695{,}552I_{10} + 239{,}360I_9 - 70{,}400I_8 + 16{,}640I_7 - 2816I_6 + 256I_5)x^8 + (631{,}488I_{12} - 329{,}472I_{11} + 160{,}512I_{10} - 71{,}808I_9 + 28{,}800I_8 - 9984I_7 + 2816I_6 - 576I_5 + 64I_4)x^6 + (-52{,}624I_{12} + 33{,}264I_{11} - 20{,}064I_{10} + 11{,}424I_9 - 6048I_8 + 2912I_7 - 1232I_6 + 432I_5 - 112I_4 + 16I_3)x^4 + (2024I_{12} - 1540I_{11} + 1140I_{10} - 816I_9 + 560I_8 - 364I_7 + 220I_6 - 120I_5 + 56I_4 - 20I_3 + 4I_2)x^2 + (-23I_{12} + 21I_{11} - 19I_{10} + 17I_9 - 15I_8 + 13I_7 - 11I_6 + 9I_5 - 7I_4 + 5I_3 - 3I_2 + I_1)\}.$$

Check:

$$G_{23}(1) = I_1 + I_2 + I_3 + I_4 + I_5 + I_6 + I_7 + I_8 + I_9 + I_{10} + I_{11} + I_{12}.$$

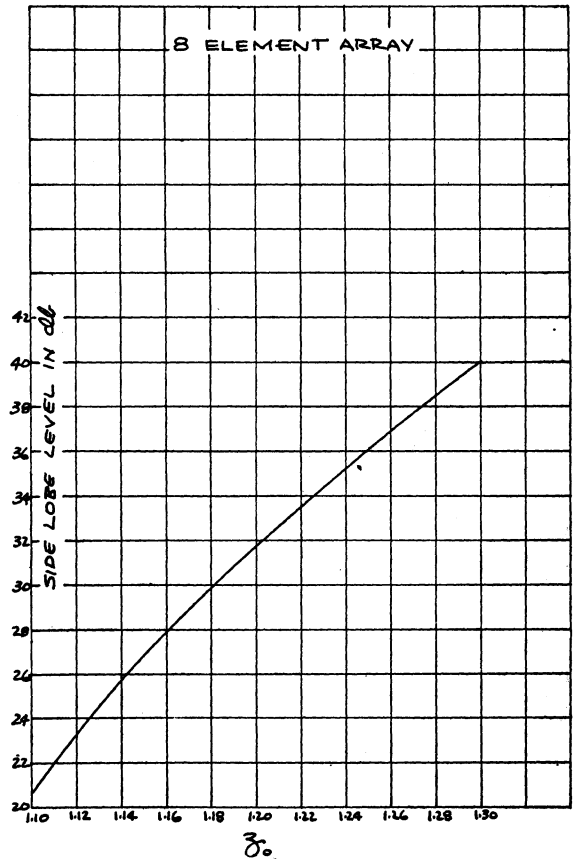

Fig. 7—The side-lobe level in decibels for "the optimum current distribution" as a function of the scale-contraction factor z_0 for an 8-element array.

Appendix III

Design Equations for

12-Element Array

$$I_6 = z_0^{11}$$

$$I_5 = 11(I_6 - z_0^9)$$

$$I_4 = 9I_5 - 44I_6 + 44z_0^7$$

$$I_3 = 7I_4 - 27I_5 + 77I_6 - 77z_0^5$$

$$I_2 = 5I_3 - 14I_4 + 30I_5 - 55I_6 + 55z_0^3$$

$$I_1 = 3I_2 - 5I_3 + 7I_4 - 9I_5 + 11I_6 - 11z_0$$

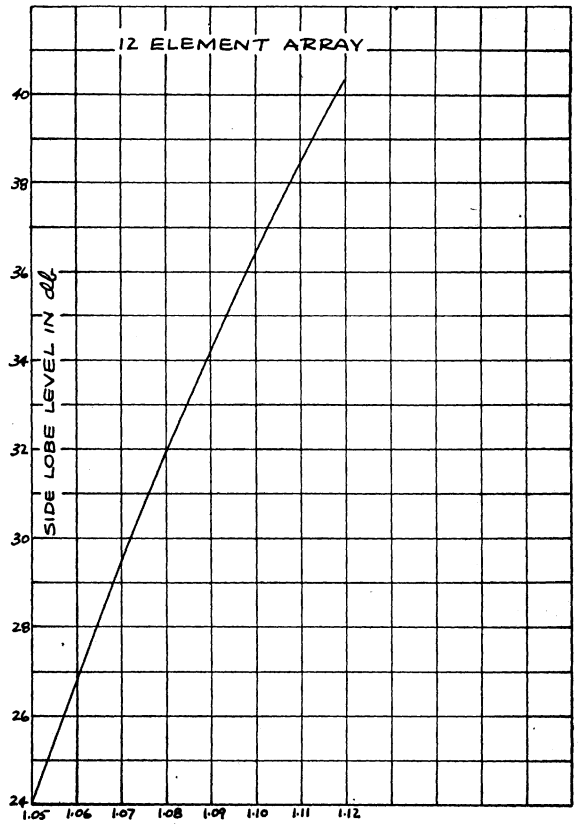

Fig. 8—The side-lobe level in decibels for "the optimum current distribution" as a function of the scale-contraction factor z_0 for a 12-element array.

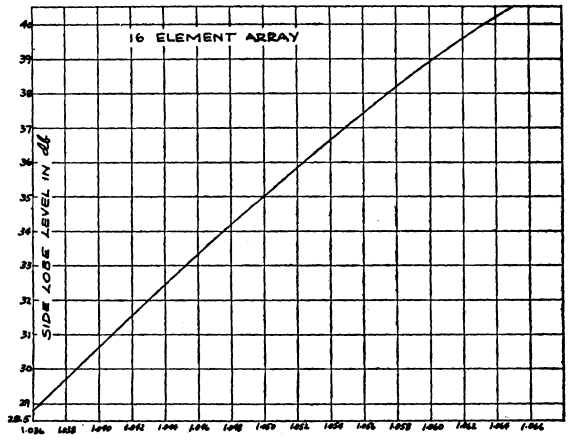

Fig. 9—The side-lobe level in decibels for "the optimum current distribution" as a function of the scale-contraction factor z_0 for a 16-element array.

16-Element Array

$$I_8 = z_0^{15}$$

$$I_7 = 15I_8 - 15z_0^{13}$$

$$I_6 = 13I_7 - 90I_8 + 90z_0^{11}$$

$$I_5 = 11I_6 - 65I_7 + 275I_8 - 275z_0^9$$

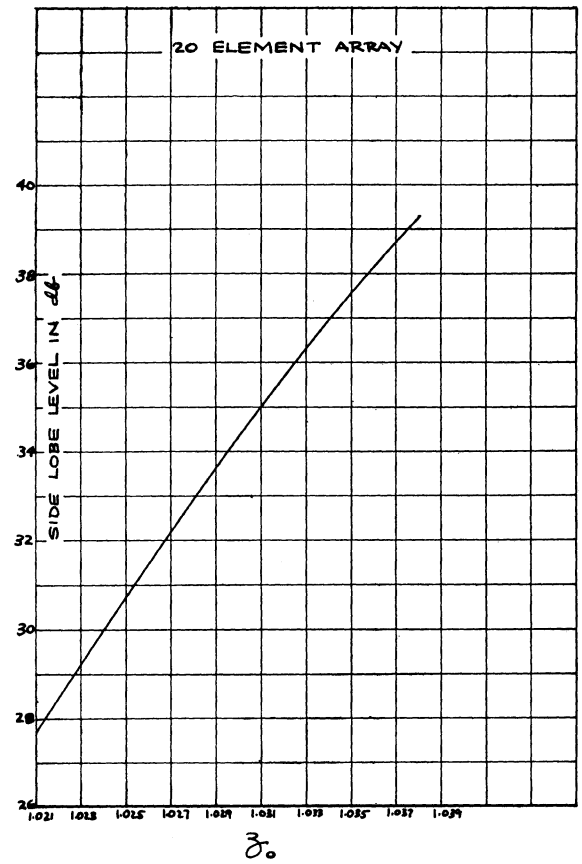

Fig. 10—The side-lobe level in decibels for "the optimum current distribution" as a function of the scale-contraction factor z_0 for a 20-element array.

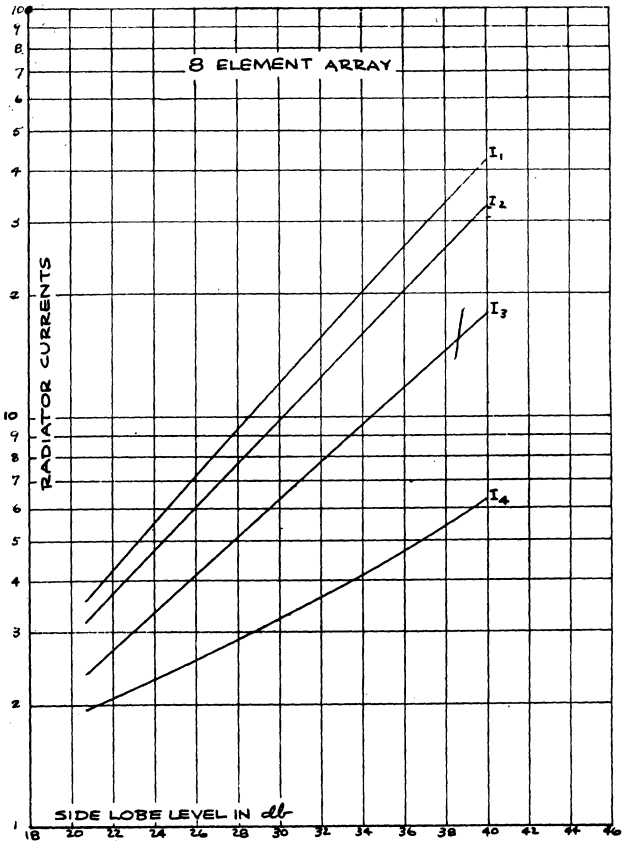

Fig. 12—The *relative* current values for an 8-element array necessary for "the optimum current distribution" as a function of side-lobe level in decibels.

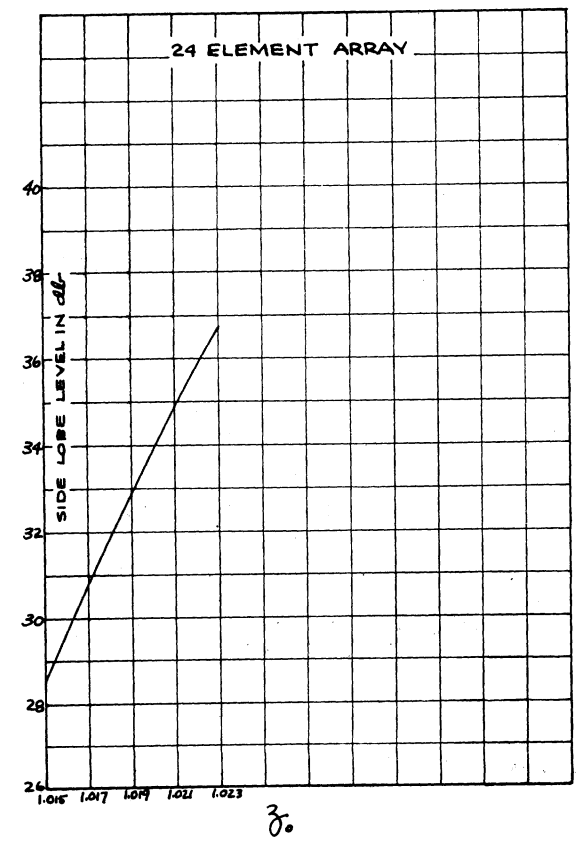

Fig. 11—The side-lobe level in decibels for "the optimum current distribution" as a function of the scale-contraction factor z_0 for a 24-element array.

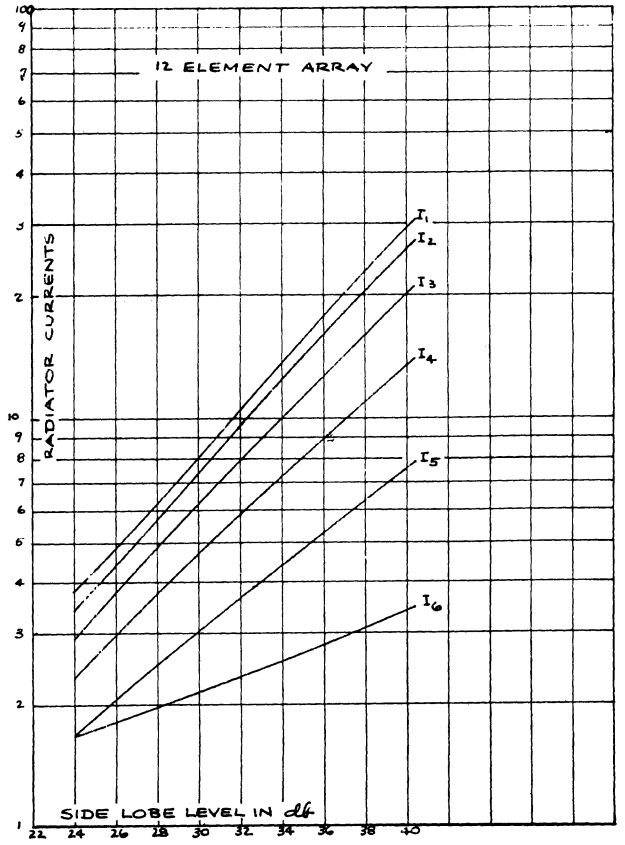

Fig. 13—The *relative* current values for a 12-element array necessary for "the optimum current distribution" as a function of side-lobe level in decibels.

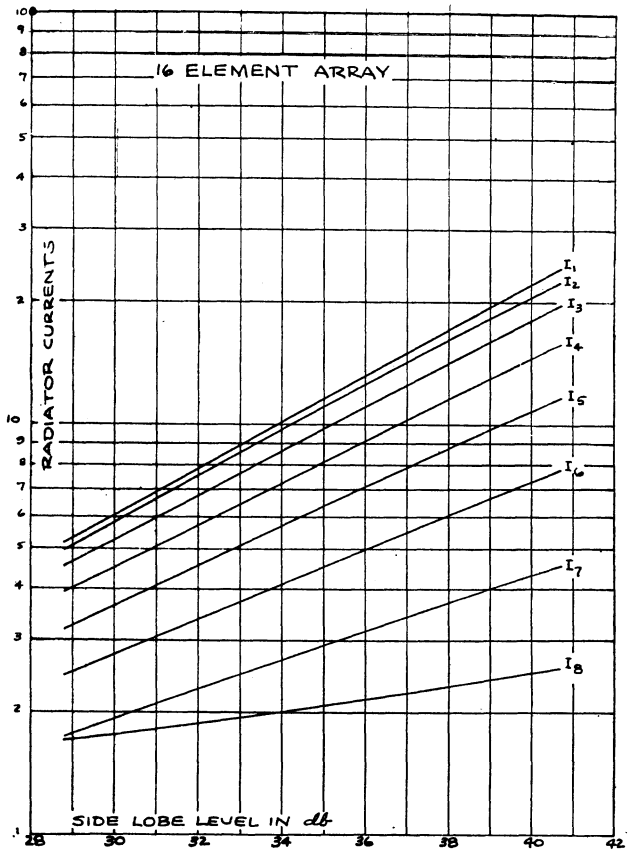

Fig. 14—The *relative* current values for a 16-element array necessary for "the optimum current distribution" as a function of side-lobe level in decibels.

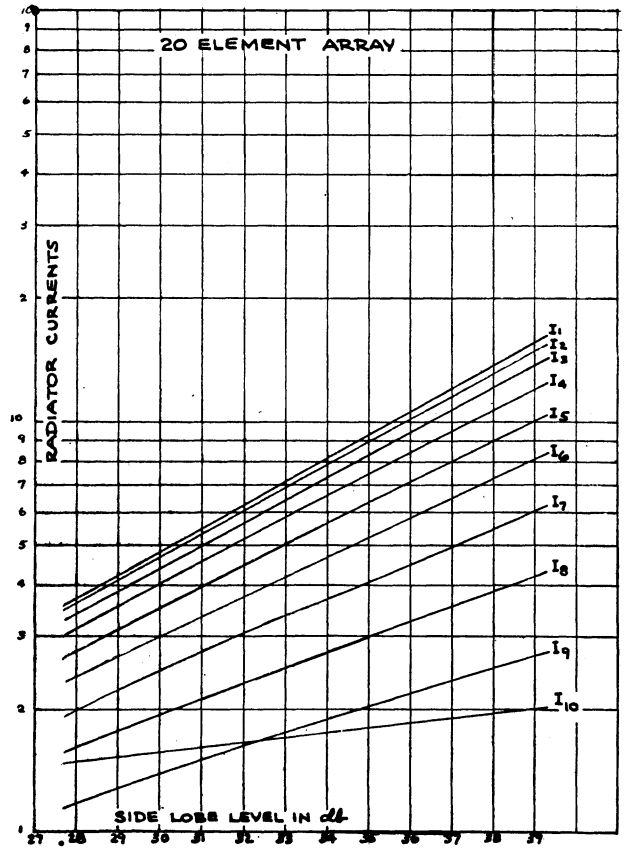

Fig. 15—The *relative* current values for a 20-element array necessary for "the optimum current distribution" as a function of side-lobe level in decibels.

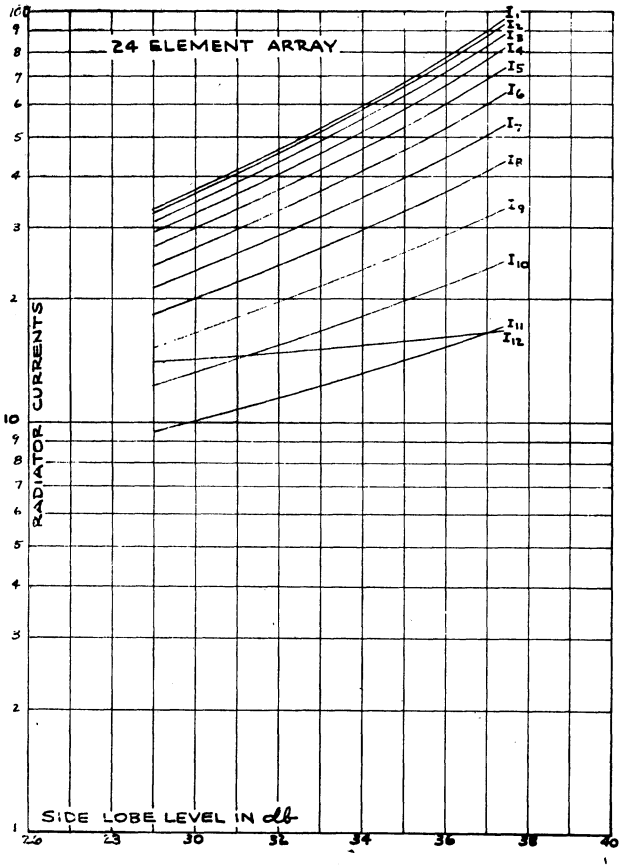

Fig. 16—The *relative* current values for a 24-element array necessary for "the optimum current distribution" as a function of side-lobe level in decibels.

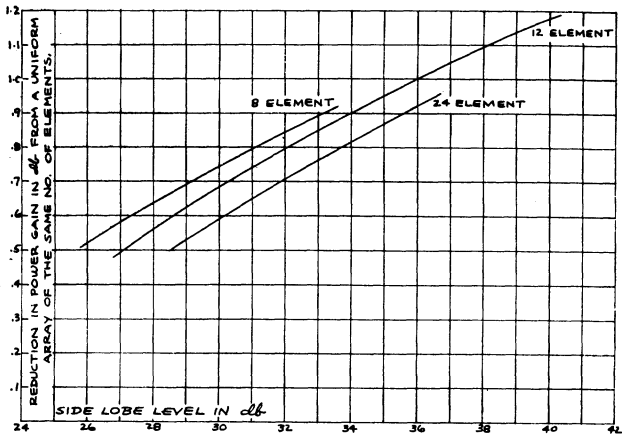

Fig. 17—The power-gain reduction of "the optimum current distribution" with respect to a "uniform" array of the same number of elements as a function of side-lobe level in decibels for 8-, 12-, and 24-element arrays, under the assumption that mutual impedances between the radiators are negligible.

$$I_4 = 9I_5 - 44I_6 + 156I_7 - 450I_8 + 450z_0^7$$

$$I_3 = 7I_4 - 27I_5 + 77I_6 - 182I_7 + 378I_8 - 378z_0^5$$

$$I_2 = 5I_3 - 14I_4 + 30I_5 - 55I_6 + 91I_7 - 140I_8 + 140z_0^3$$

$$I_1 = 3I_2 - 5I_3 + 7I_4 - 9I_5 + 11I_6 - 13I_7 + 15I_8 - 15z_0.$$

20-Element Array

$$I_{10} = z_0^{19}$$
$$I_9 = 19I_{10} - 19z_0^{17}$$
$$I_8 = 17I_9 - 152I_{10} + 152z_0^{15}$$
$$I_7 = 15I_8 - 119I_9 + 665I_{10} - 665z_0^{13}$$
$$I_6 = 13I_7 - 90I_8 + 442I_9 - 1729I_{10} + 1729z_0^{11}$$
$$I_5 = 11I_6 - 65I_7 + 275I_8 - 935I_9 + 2717I_{10} - 2717z_0^9$$
$$I_4 = 9I_5 - 44I_6 + 156I_7 - 450I_8 + 1121I_9 - 2508I_{10} + 2508z_0^7$$
$$I_3 = 7I_4 - 27I_5 + 77I_6 - 182I_7 + 378I_8 - 714I_9 + 1254I_{10} - 1254z_0^5$$
$$I_2 = 5I_3 - 14I_4 + 30I_5 - 55I_6 + 91I_7 - 140I_8 + 204I_9 - 285I_{10} + 285z_0^3$$
$$I_1 = 3I_2 - 5I_3 + 7I_4 - 9I_5 + 11I_6 - 13I_7 + 15I_8 - 17I_9 + 19I_{10} - 19z_0.$$

24-Element Array

$$I_{12} = z_0^{23}$$
$$I_{11} = 23I_{12} - 23z_0^{21}$$
$$I_{10} = 21I_{11} - 230I_{12} + 230z_0^{19}$$
$$I_9 = 19I_{10} - 189I_{11} + 1311I_{12} - 1311z_0^{17}$$
$$I_8 = 17I_9 - 152I_{10} + 952I_{11} - 4692I_{12} + 4692z_0^{14}$$
$$I_7 = 15I_8 - 119I_9 + 665I_{10} - 2940I_{11} + 10{,}948I_{12} - 10{,}948z_0^{13}$$
$$I_6 = 13I_7 - 90I_8 + 442I_9 - 1729I_{10} + 5733I_{11} - 16{,}744I_{12} + 16{,}744z_0^{11}$$
$$I_5 = 11I_6 - 65I_7 + 275I_8 - 935I_9 + 2717I_{10} - 7007I_{11} + 16{,}445I_{12} - 16{,}445z_0^9$$
$$I_4 = 9I_5 - 44I_6 + 156I_7 - 450I_8 + 1122I_9 - 2508I_{10} + 5148I_{11} - 9867I_{12} + 9867z_0^7$$
$$I_3 = 7I_4 - 27I_5 + 77I_6 - 182I_7 + 378I_8 - 714I_9 + 1254I_{10} - 2079I_{11} + 3289I_{12} - 3289z_0^5$$
$$I_2 = 5I_3 - 14I_4 + 30I_5 - 55I_6 + 91I_7 - 140I_8 + 204I_9 - 285I_{10} + 385I_{11} - 506I_{12} + 506z_0^3$$
$$I_1 = 3I_2 - 5I_3 + 7I_4 - 9I_5 + 11I_6 - 13I_7 + 15I_8 - 17I_9 + 19I_{10} - 21I_{11} + 23I_{12} - 23z_0.$$

Appendix IV

The accompanying design curves are shown for broadside, symmetric arrays of 8, 12, 16, 20, and 24 elements over an approximate side-lobe-level range of 26 to 40 decibels.

Figs. 7, 8, 9, 10, and 11 are useful in estimating beam widths to half-power points.

Figs. 12, 13, 14, 15, and 16 give the *relative* current values needed in design.

Fig. 17 is useful in predicting power-gain performance.

High-Impedance Cable*

HEINZ E. KALLMANN†, SENIOR MEMBER, I.R.E.

***Summary*—A cable with an impedance of the order of 1000 ohms is described. It resembles the usual flexible concentric cable with a 3/8-inch outside diameter, but its inner conductor is a single-layer coil continuously wound on a flexible core of 0.110-inch diameter. The cable is suitable for video connections from chassis to chassis and to remote indicators.**

PRESENT types of video amplifiers are built with load impedances of the order of 1000 ohms; the cables, however, now used for video signals have impedances of 50 to 100 ohms, with capacitances of 30 to 100 micromicrofarads per meter. They may be matched to correspondingly low load resistances, or they may be treated as lumped load capacitances, in either case enforcing low gain and low peak-voltage output available from a given tube.

* Decimal classification: R117.2×R282.1. Original manuscript received by the Institute, January 7, 1946; revised manuscript received, February 27, 1946. This paper is based on work done for the Office of Scientific Research and Development under contract OEMsr-262 with the Radiation Laboratory, Massachusetts Institute of Technology. The cable described herein was subsequently produced by the Federal Telephone and Radio Corporation under contract OEMsr-1283.

† Formerly, Radiation Laboratory, Massachusetts Institute of Technology, Cambridge, Massachusetts; now, consulting engineer, New York, N. Y.

To avoid these losses, cables having much higher surge impedances are desirable. A suitable design can be derived from that used for delay lines of the distributed-parameter type, but with dimensions modified so as to yield the high impedance Z_0 with the least possible signal delay and attenuation per unit length. To this end, the inductance L per unit length is increased, while the capacitance C is kept low, since

$$Z_0 = \sqrt{L/C} \text{(ohms, henries, farads)}. \quad (1)$$

An experimental cable was made, resembling a low-capacitance concentric cable except that the inner conductor was a small-diameter single-layer coil, continuously wound on a flexible core, as shown with dimensions in Figs. 1 and 2. The core, 0.060-inch thick, was made of Saran, a moderately flexible plastic; the inner conductor was close-wound on it with No. 34 HF Formex wire. A helix wound from 0.065-inch polystyrene with 0.15-inch pitch was used as a spacer, with an outer diameter of about 0.25 inch. The outer conductor was 3/16-inch braid of 175 tinned 0.005-inch copper wires. The cable, with an outside diameter of 5/16 inch, can be bent to a 2-inch diameter circle.